Supplementary Material

Structural Optimization of Lightweight Electric Vehicle Spaceframe Chassis Under Variable Payload Distributions

Ashwin Swamy

Supplementary Table S1 — Mesh convergence, all three load cases

Load case	Chassis	Step 1 elem.	Step 2 elem.	Disp. 1 (mm)	Disp. 2 (mm)	Δ (%)
Torsion (1000 N/side)	Semi-spaceframe	139,292	161,408	0.476	0.472	0.85
Torsion (1000 N/side)	Ladder frame	28,395	44,449	20.96	20.63	1.61
Asymmetric (800 kg)	Semi-spaceframe	139,292	200,637	0.573	0.572	0.18
Asymmetric (800 kg)	Ladder frame	28,395	31,899	17.05	16.80	1.45
Symmetric (800 kg)	Semi-spaceframe	139,292	200,878	0.299	0.299	0.18
Symmetric (800 kg)	Ladder frame	28,395	33,255	11.04	10.90	1.30

Peak displacement between successive mesh refinements. All six combinations change by less than the 2% criterion between the two finest meshes. Displacements are raw solver output, before the β correction.

Model and load case	Nodes	DOF	Element edge length (mm)
Semi-spaceframe, torsion	307,462	922,386	0.67–29.8
Semi-spaceframe, asymmetric	376,968	1,130,904	0.055–28.7
Semi-spaceframe, symmetric	377,361	1,132,083	0.055–28.7
Ladder frame, torsion	83,968	251,904	1.26–26.8
Ladder frame, asymmetric	61,154	183,462	2.26–35
Ladder frame, symmetric	63,606	190,818	1.88–35

Final converged mesh for each model and load case.

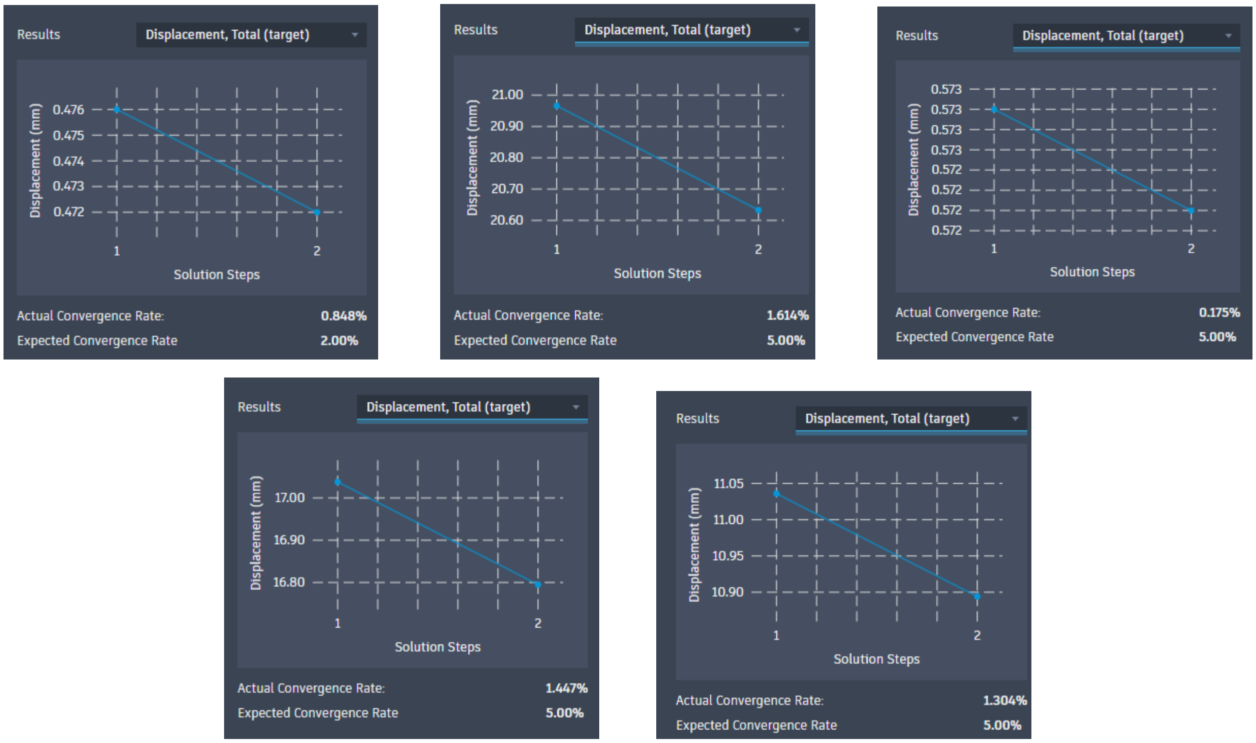

Figure S1. Fusion 360 adaptive-refinement convergence output for the mesh studies summarised in Table S1: semi-spaceframe and ladder frame under torsion (top left, top centre), semi-spaceframe and ladder frame under asymmetric payload (top right, bottom left), and ladder frame under symmetric payload (bottom right). Each plot shows the target displacement across successive refinement steps together with the achieved convergence rate. Numerical values for all six combinations, including the semi-spaceframe symmetric case, are given in Table S1.

Supplementary Table S2 — Constraint-point stress probes

Local mesh length (mm)	Peak nodal σ (MPa)	Hot-spot σ at 30 mm (MPa)	Nominal member σ (MPa)
Semi-spaceframe, asymmetric payload			
12.0	242	118	98.4
6.0	318	113	97.4
3.0	389	113	99.0
Ladder frame, asymmetric payload			
12.0	988	811	173
6.0	1068	820	177
3.0	1544	810	182
Ladder frame, symmetric payload			
12.0	559	466	129
6.0	604	459	136
3.0	873	453	135

In every case the peak nodal stress rises monotonically with refinement and is classified as singular. The hot-spot stress converges in all three: 115 MPa for the semi-spaceframe (factor of safety 2.17 against the 250 MPa yield), 815 MPa for the ladder frame under asymmetric load (3.3× yield) and 455 MPa under symmetric load (1.8× yield). The ladder frame therefore yields locally at the joint while its members remain moderately loaded.

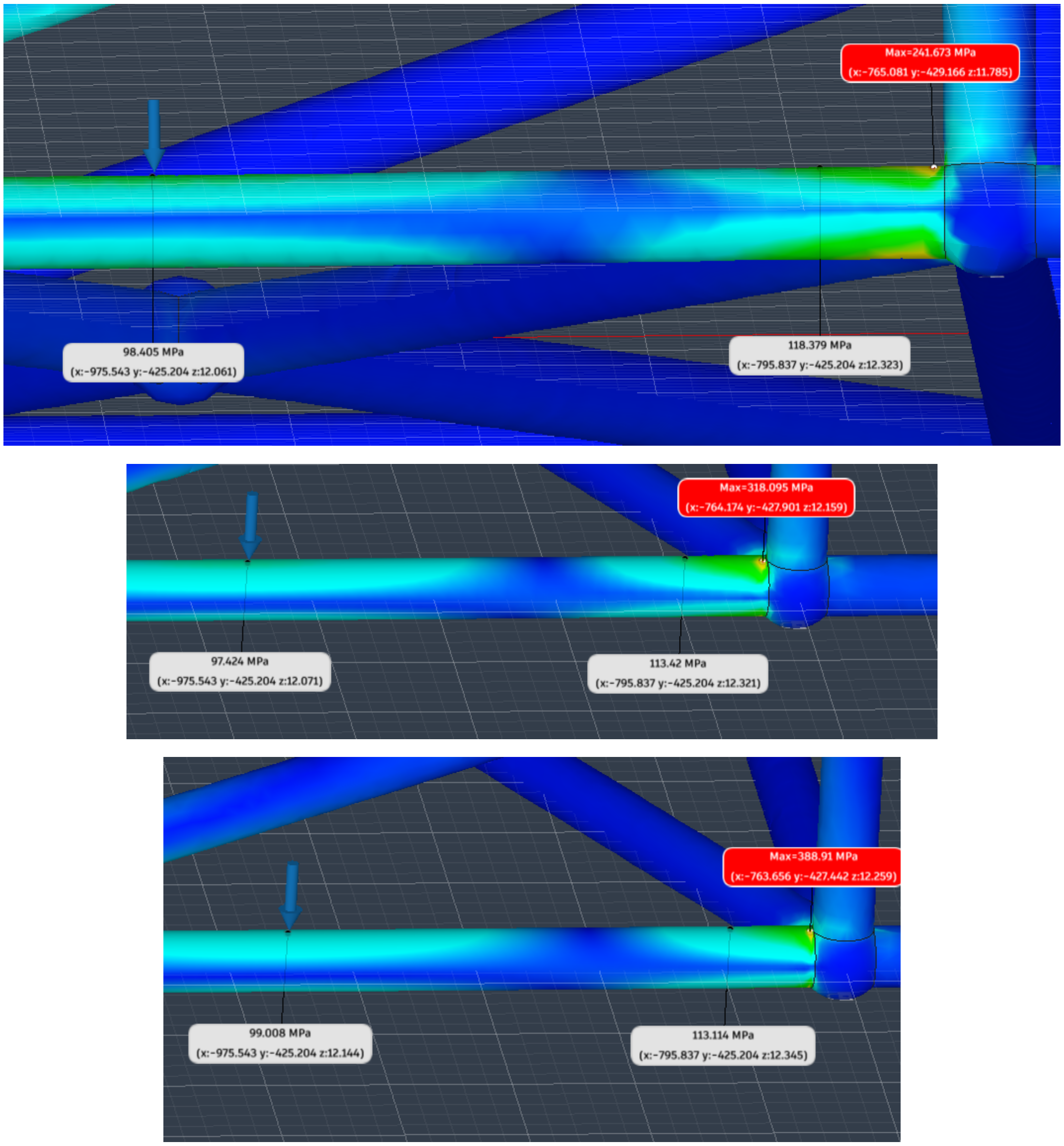

Figure S2. Local mesh refinement at the constrained node of the semi-spaceframe under asymmetric payload, at local element lengths of 12.0 mm (top), 6.0 mm (middle) and 3.0 mm (bottom). The three probes in each view correspond to the three columns of Table S2: the peak nodal stress at the constraint itself, the hot-spot stress one tube diameter (30 mm) away, and the nominal stress at member mid-length. The peak nodal value rises with refinement while the hot-spot and nominal values remain effectively constant, which is the basis for classifying the peak as a singularity.

Supplementary Table S3 — Matched track-width comparison (both chassis at 850 mm)

Metric	Ladder frame	Semi-spaceframe	Ratio
Asymmetric payload, 800 kg			
Corrected max sag (mm)	31.5	1.35	23.3×
Induced twist angle (deg)	2.12	0.0910	23.3×
Max von Mises stress (MPa)	942.2	222.3	—
Symmetric payload, 800 kg			
Corrected max sag (mm)	20.3	0.708	28.7×
Max von Mises stress (MPa)	532.4	110.3	—

Re-run with both chassis constrained at a common 850 mm track and the suspension architecture removed, so the comparison is not influenced by the wider as-built semi-spaceframe track. Induced twist rises only from 0.0858 to 0.0910 deg relative to the as-built configuration, and the sag and twist ratios agree at 23.3×.

Supplementary Table S4 — Solid-proxy vs hollow-tube sensitivity

Quantity (ladder-frame substructure)	Solid-proxy + α/β	Hollow tube	Difference
Torsional stiffness K (Nm/deg)	39.6	46.7	15%
Asymmetric max sag (mm)	31.5	28.8	9.0%
Asymmetric induced twist (deg)	2.12	1.94	8.9%
Symmetric max sag (mm)	20.3	21.5	5.7%

The ladder-frame structure was used because it is a substructure common to both chassis and meshes cleanly as hollow tube. The corrected solid-proxy model agrees with the true hollow-tube model to within 15% across all three load cases. The deviations are not all in the same sense: the correction understates torsional stiffness and symmetric sag, and overstates asymmetric sag and twist.

Force per side (N)	Total twist displacement (mm)	Torque (Nm)	θ_{real} (deg)
500	35.4	212.5	4.76
1000	70.8	425	9.46
1500	106	637.5	14.0
2000	141	850	18.4

Hollow-tube ladder-frame torsional response. Linear regression of torque against corrected twist angle gives $K = 46.7$ Nm/deg with $R^2 = 0.9998$.

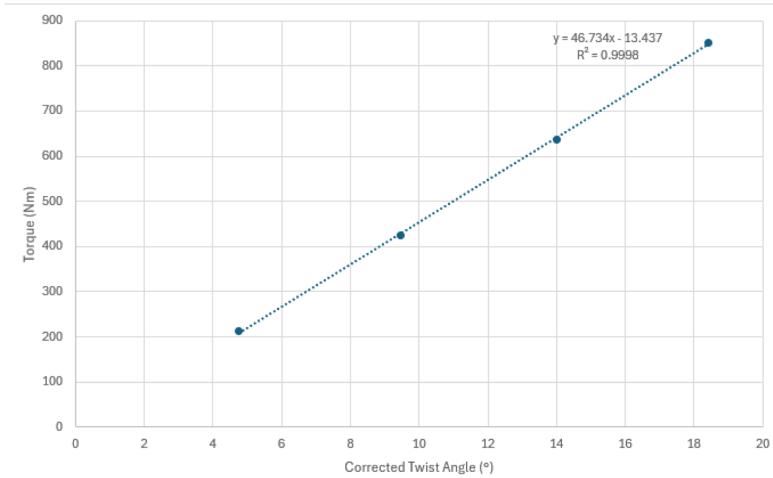

Figure S3. Torque against corrected twist angle for the true hollow-tube ladder-frame substructure, giving $K = 46.7$ Nm/deg. This is the hollow-tube reference against which the corrected solid-proxy value of 39.6 Nm/deg is compared in Table S4.